Novel adaptive finite element algorithms to predict bone ingrowth in additive manufactured porous implants

Vee San Cheong [a,b,]*, Paul Fromme [b], Aadil Mumith [a], Melanie J. Coathup [a], Gordon W. Blunn [a,c]

a John Scales Centre for Biomedical Engineering, Institute of Orthopaedics and Musculoskeletal Science, University College London, Royal National Orthopaedics Hospital, Stanmore HA7 4LP, UK

b Department of Mechanical Engineering, University College London, London WC1E 7JE, UK

c School of Pharmacy and Biomedical Sciences, University of Portsmouth, Portsmouth PO1 2DT, UK

* Corresponding author

Email: v.cheong@ucl.ac.uk

Tel: +44 (0)20 7679 3944

Fax: +44 (0)20 7388 0180

Declarations of interest: None

1

Abstract

Bone loss caused by stress shielding of metallic implants is a concern, as it can potentially lead to long-term implant failure. Surface coating and reducing structural stiffness of implants are two ways to improve bone ingrowth and osteointegration. Additive manufacturing, through selective laser sintering (SLS) or electron beam melting (EBM) of metallic alloys, can produce porous implants with bone ingrowth regions that enhance osteointegration and improve clinical outcomes. Histology of porous Ti6Al4V plugs of two pore sizes with and without electrochemically deposited hydroxyapatite coating, implanted in ovine condyles, showed that bone formation did not penetrate deep into the porous structure, whilst significantly increased bone growth along coated pore surfaces (osteointegration) was observed. Finite Element simulations, combining new algorithms to model bone ingrowth and the effect of surface modification on osteoconduction, were verified with the histology results. The results showed stress shielding of porous implants made from conventional titanium alloy due to material stiffness and implant geometry, limiting ingrowth and osteointegration. Simulations for reduced implant material stiffness predicted increased bone ingrowth. For low modulus Titanium-tantalum alloy (Ti-70%Ta), reduced stress shielding and enhanced bone ingrowth into the porous implant was found, leading to improved mechanical interlock. Algorithms predicted osteoconductive coating to promote both osteointegration and bone ingrowth into the inner pores when they were coated. These new Finite Element algorithms show that using implant materials with lower elastic modulus, osteoconductive coatings or improved implant design could lead to increased bone remodelling that optimises tissue regeneration, fulfilling the potential of enhanced porosity and complex implant designs made possible by additive layer manufacturing techniques.

Keywords: osteointegration, osteoconduction, porous scaffold, implant design, finite element analysis, biomaterial coating

1.   Introduction

The treatment of patients with major bone loss, due to trauma or tumour, using traditional implant designs, is often difficult due to the limited quality and quantity of bone stock remaining [1, 2]. In segmental bone defects of the proximal femur, a massive implant is often used to replace the femoral metaphysis and part of the diaphysis. The physical demands on these implants are high, leading to aseptic loosening as the main mode of implant failure. In these cases, extracortical bony bridging and ingrowth, where bone grows from the transection site onto the surface of the implant to achieve osteointegration, improves the survivorship of implants at 10 years from 75 to 98 % [3]. Finite element analysis (FEA) showed that this improved bone ingrowth results in a reduction in fracture risk of the implant stem, and a more natural stress distribution to the bone [2, 4].

Bone ingrowth and osteointegration is a multifactorial process involving implant surface area, bioactivity of the substrate, and mechanical properties [5]. Titanium alloy (Ti6Al4V) is routinely used as an implant material due to its high fatigue strength, capacity for osteointegration, bio-inertness and corrosion resistance [6]. Recent advances in electron beam melting (EBM) and selective laser sintering (SLS) (additive manufacturing) have enabled the fabrication of porous implants using Ti6Al4V that can result in bone ingrowth of up to 56% [7, 8]. Porous structures have lower structural stiffness, reducing the mismatch between the implant and the adjacent bone [7, 9]. The reduction of overall structural stiffness of the implant improves the mechanical stimulus for bone regeneration and reduces the effect of stress shielding [10, 37]. Ti6Al4V has an elastic modulus that is 10 times higher than that of cortical bone and new porous, low modulus Titanium alloys which are now available, can potentially increase bone ingrowth further [9, 10].

Surface modification of implants using biomimetic materials improves biological response and bone-implant fixation [11, 12], through preferential osteoblastic differentiation along the coated surfaces (osteoconduction). Usually these coatings are applied using a 'line of site" process (plasma spraying), but in substantially porous structures, only the outer pore surfaces will be treated. An alternative

method is via solution based calcium phosphate coatings, but these have shown mixed results. The amount of bone ingrowth did not significantly change for mandibular defects [8], but did significantly increase in femoral diaphyseal defect implants [11]. The loading conditions are different for the two implant sites, suggesting that the contribution of surface modification to improve osteointegration may depend on the loading conditions, especially when porous additively manufactured scaffolds are used. Electrochemical coating of porous implant scaffolds, made using SLS with hydroxyapatite (HA), resulted in significantly increased bone ingrowth into implants [13, 14]. Therefore, the contribution of surface coating combined with the geometry of the pores and the modulus of the material should be considered for the design or analyses of extensive porous implants made using additive manufacturing. In order to reduce the reliance of testing in animals, predictive models are required.

Static FEA models evaluate the performance of implants by assessing the mechanical environment for bone adaptation at the initial stage after surgery. However, the load carried by the bone increases with bone ingrowth, affecting the mechanical stimulus for further bone remodelling in the porous biomaterials [15]. In order to obtain information about the remodelling process, adaptive bone simulations are preferred, especially for the long-term performance of the implant [16, 17]. Moreover, these simulations can be used to determine the optimum implant design for each site, as they are application-specific [18]. Several methods have been developed to model the remodelling process, including the use of continuum damage mechanics, mechanoregulatory algorithms, daily stress, and adaptive elasticity theory. Strain energy density (SED) is commonly used as the remodelling stimulus, comparing the stimulus value against a reference value, and is directly correlated with changes in bone density [19-21]. Changes in bone density around an implant have been predicted for internal remodelling [16, 22, 23] and are associated with changes in bone density rather than changes in bone shape. Bone ingrowth in porous implants has been modelled to predict remodelling at equilibrium state [17, 22, 24], but yield little information on the progression of bone formation associated with adaptive shape changes, which has been observed clinically as

4

extracortical bone formation adjacent to segmental prosthesis. Current algorithms based on SED are not able to predict the progression of bone ingrowth into substantially porous structures made by additive manufacturing. To predict the progression of external bone formation in segmental prostheses, a connectivity matrix was used to control the sequential laying down of new bone in a soft tissue envelope of elements (so called osteoconnectivity), around a grooved implant collar, giving improved time correspondence with clinical results [25]. However, the contribution of the presence of coating has not been modelled in porous or textured implants. The effect of pore size and material properties have not been optimised for bone ingrowth and osteointegration of substantially porous implants made by additive manufacturing. Furthermore, an *in vivo* study has shown that an implant design that is optimised by assuming the presence of osteointegration may not be valid, as the animal study showed only localised bone apposition along the uncoated implant surface [26, 27]. Bone ingrowth occurred throughout the coated implant, indicating the importance of combining the response to a surface that imparts bioactivity with the osteoconnectivity in an FE model. This shows the importance of developing a FEA model that can predict the amount of bone ingrowth and osteointegration.

The main aim of this study was to understand how to achieve osteointegration and ingrowth in porous implants, and optimise them using HA coating, geometry (pore size), and material properties to maximise bone formation and osteointegration. This study quantified stress shielding and bone ingrowth based on implant design and material. The contribution of osteoconductive coating in increasing osteointegration and bone formation is modelled, by varying parameters of the osteoconnectivity algorithm of bone adaptation developed for extracortical bone formation, and verifying them with data observed in the experimental studies. The contribution of coating has not been modelled previously for porous or textured implants. The use of the osteoconnectivity model is suitable to model bone formation in the critical size defect model as bone growth is largely intramembranous, similar to extracortical bone formation in a segmental prosthesis. To achieve these aims, the remodelling results predicted by the FEA models were verified with histology results

of Ti6Al4V plugs of two pore sizes implanted into trabecular bone. In the FEA model, the material properties of the implant and presence of coating were varied to determine if the implant performance could be improved.

2.   Materials and methods

2.1. Animal model

Porous SLS scaffolds with pore sizes of 700 and 1500 μm were designed, manufactured, and tested *in vivo* in a mature ovine femoral condyle critical-size defect model (Fig. 1) as part of a larger study of the parameters that affect bone ingrowth. The ingrowth of bone with and without the presence of hydroxyapatite coatings was investigated [13]. The two pore sizes were incorporated into one implant, with 8 mm diameter and 14.5 mm length. Bilateral critical size defects were created in the medial femoral condyles of both the right and left hind limbs of 6 sheep. The implants were press-fitted, the remaining tissues and periosteum repaired and the sheep allowed to recover with unrestricted weight bearing. Animal care and all procedures were carried out in accordance to the UK Animals (Scientific Procedures) Act 1986, under personal and project licences from the UK Home Office following review by the local animal welfare and ethical research committee.

The implants were retrieved for histological analysis after 6 weeks. Excess soft tissue was removed and fixed in formalin before the specimens were dehydrated. The plug implants were then embedded in hard grade acrylic resin and sectioned longitudinally to obtain thin sections approximately 80 μm thick to yield a total of 6 slices each for the coated and uncoated implants. The sections were stained in Toluidine Blue and Paragon to identify soft tissue and bone respectively. Stained slides were imaged under a light microscope (Axioskop, Carl Zeiss, Welwyn Garden City, UK). The surface integration was determined by importing the images into ImageJ (v1.51, National Institute of Health, Bethesda, USA), and the length of implant with direct bone contact measured and normalised by the total implant surface length, using thresholding and freeform methods.
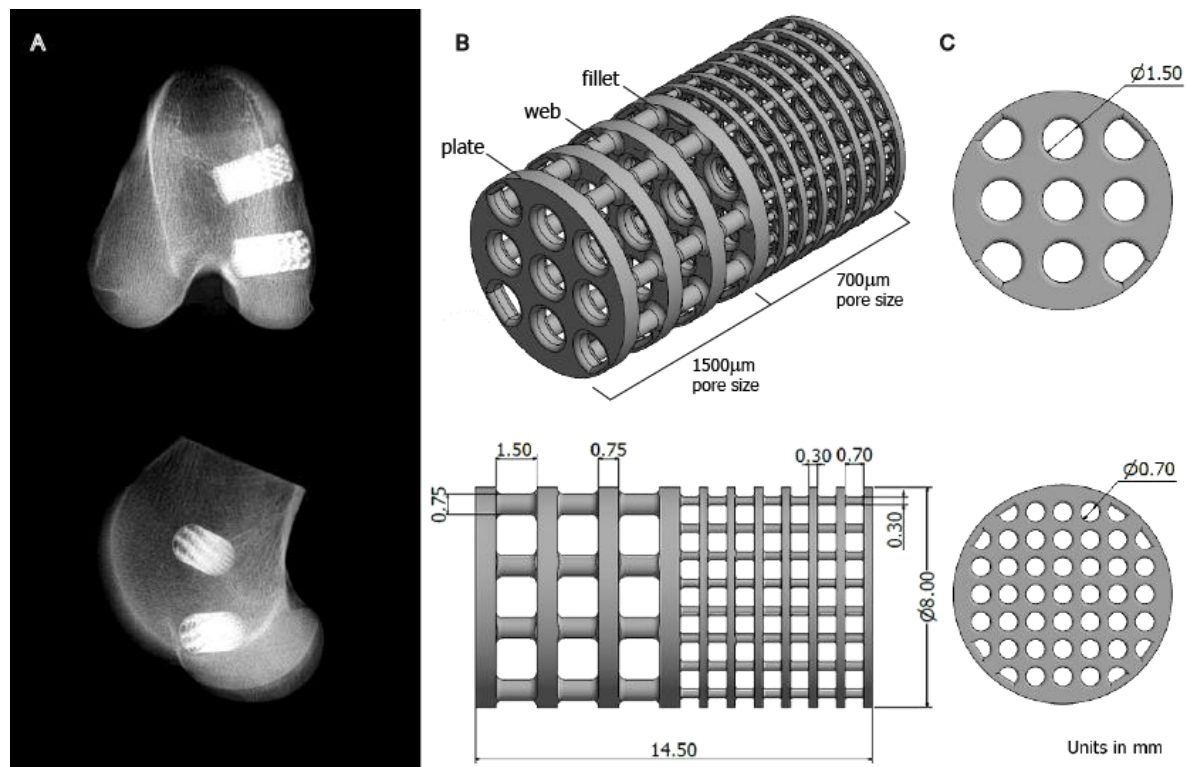
Fig. 1. (A) Radiographs of the implanted porous scaffolds (14.5 mm length, 8 mm diameter). (B) 3D solid models. (C) Transverse cuts taken across the plates; dimensions in mm.

2.2. Finite element analysis

Separate FEA models of the implant with the two pore sizes were developed with the plug implanted in trabecular bone as in the experiments. Using rotational symmetry, geometry, and repeating patterns, only a quarter slice was simulated to reduce computational cost (Fig. 2). The 1500 μm pore size quarter model had dimensions of 5 mm x 5 mm x 2.25 mm and was loaded by a uniform diametric pressure load of 200 N, corresponding to the peak axial force of 2.25 body weight (BW) in ovine stifle [28]. Axial loading was applied, as in vivo data combined with musculoskeletal modelling conducted in ovine stifle joint showed that the bending components accounted for less than 20% of the axial force [28], and would be negligible in the condyles of the knees where normal force is predominately transmitted. The 700 μm pore size model measured 5 mm x 5 mm x 1 mm. A 88.9 N load was used for the 700μm model, scaled according to the width. The 1500 and 700 μm models

have porosities of 70% and 75% respectively. Tied nodal contact was assumed throughout the model. The bone and the titanium plug were modelled with isotropic homogenous material properties (Bone: Elastic modulus E = 1.5 GPa, Poisson's ratio v = 0.34; Ti6Al4V: 110 GPa, v = 0.34) [28]. Soft tissue of uniform initial modulus (0.5 GPa, v = 0.3) was assumed to fill the volume within the plug [19]. Static stress analysis was conducted to investigate mesh convergence. The geometries were meshed using linear tetrahedral elements for the soft tissue and linear hybrid mesh for bone and titanium (Fig. 2B) for improved geometrical conformity. The solution converged for mesh sizes of 0.06 mm and 0.03 mm (≤5 % stress change at fillet and ≤1 % for soft tissue), leading to 1.33 million and 2.78 million elements for the 1500 and 700 µm plug models respectively.
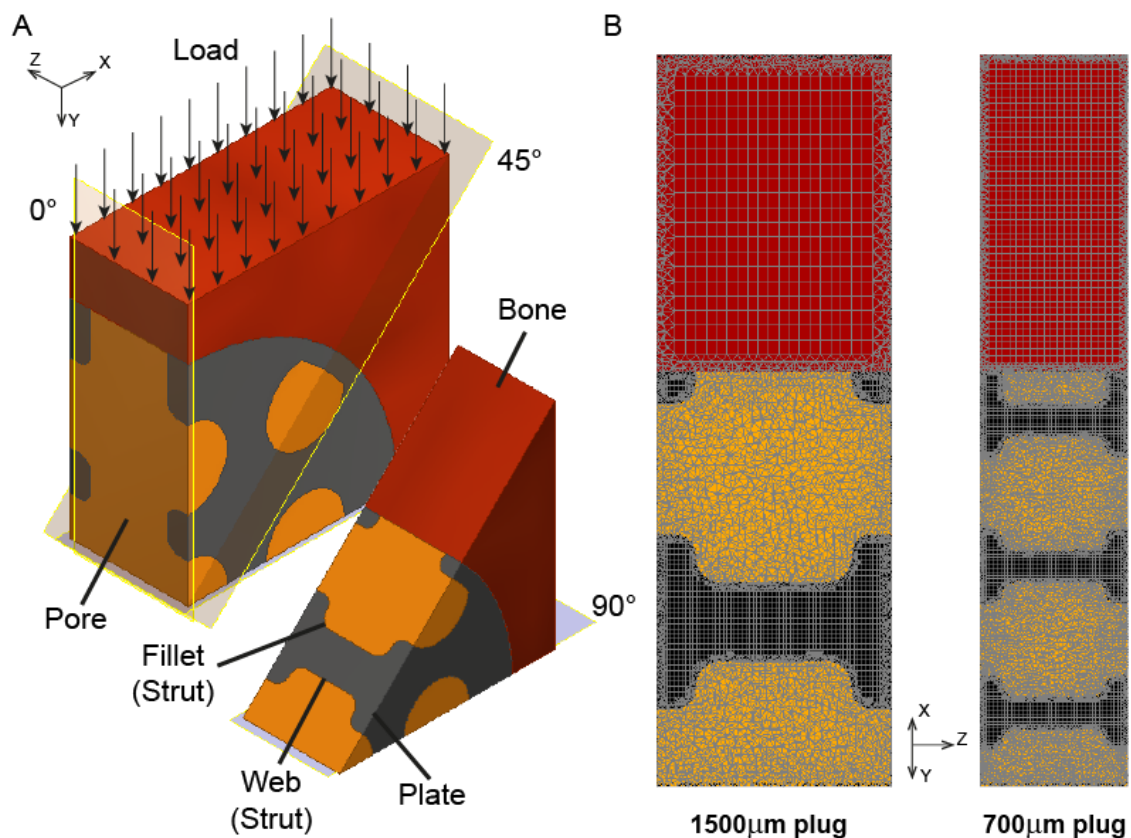

Fig. 2. (A) Schematic representation of the quarter FEA model of 1500 µm plug, 45⁰ cut shown. (B) FEA mesh of cut taken at 45⁰ from the load direction for 1500 and 700 µm plug. Pores are indicated in orange and refer to all connected soft tissue space within the implant. Plates and struts run parallel and perpendicular to the loading direction respectively.

A parametric study was conducted by varying the material properties of the plug models to investigate bone remodelling for different implant materials. Ti-70% Ta alloy (67 GPa) [29], and PEEK (3.8 GPa) were selected as reference values; additionally material properties were varied in the model using 50 (Ti-Ni), 40, and 25 GPa. The Poisson's ratio was defined as 0.34 for all materials except as 0.38 for PEEK.

2.3. Bone remodelling simulation

The enhanced 3D bone formation and adaptation model, termed osteoconnectivity, was used to predict the changes in bone formation and understand the growth process [25]. The algorithm was developed for intramembranous bone growth, which is applicable for the critical size defect ovine model. The model enforces that remodelling of bone occurs only adjacent to existing bone and subsequent remodelling of bone occurs next to elements that have begun adapting at a previous time step. This concept, named here as connectivity, is different from the standard adaptive elasticity theory and most other mechanotransduction algorithms that permit all elements to adapt concurrently or add elements at the periosteal surface. The osteoconnectvity model is based on the adaptive elasticity theory, where bone adaptation is driven by strain energy density (SED) per unit mass [19, 30]:

$$(1 - \delta)k \leq SED \leq (1 + \delta)k \tag{1}$$

A reference value of 0.004 Jg^{-1} was used for k, the critical SED. The dead zone where no remodelling occurs was assigned a 10% bandwidth for δ [19]. When the SED is lower or higher than the dead zone, the tissue density changes via resorption or apposition respectively. The change in density was computed using Eq. 2, and used to update the stiffness matrix using a density-modulus relationship ($E = 3790\rho^3$) [31]. The remodelling rate B was set as $1 gcm^{-3}$ based on literature data [19]. An upper threshold for bone formation ρ_{cb}, was set as corresponding to 12GPa, the average elastic modulus of the trabeculae [32]. Additionally, a conductivity algorithm was developed and used to model the

effect of osteoconduction in coated implants, by modifying the remodelling law to preferentially allow soft tissues in contact with the coated implant surfaces to form bone. The levels of tissue strain required for bone to form was reduced for the elements adjacent to the implant surface. k was set at 0 Jg^{-1} with no bandwidth ($\delta = 0$), and a remodelling rate B of 5 gcm^{-3} was assumed, to model the increased bone formation due to the osteoconductive coating, lowering the threshold SED and increasing the remodelling rate:

$$\frac{d\rho}{dt} = B(SED - k) \quad 0 < \rho \leq \rho_{cb} \tag{2}$$

The simulations were conducted using an initial fixed, non-dimensional time step of 0.1 computer time units (ctu) until the number of remodelling elements remained unchanged, at time = 50 ctu. Thereafter, adaptive stepping at 1.2x of the previous step was used, for computational efficiency, as the rate of change slows asymptotically towards equilibrium, e.g. bone density increased by 6.4% from 100 ctu to 1000 ctu. For humans it was found previously that a ctu of 4.0 corresponds approximately to 1 year [25]. However, the time correspondence for sheep has not been established in literature and for this study, histology results were only available at one time point, after 6 weeks. The iterative simulations were conducted using the FEA software MSC.Marc 2017.0 (MSC Software Corporation, Santa Ana, CA, USA).

2.4. Verification of FEA models

The FEA predictions for two models with different pore sizes, with and without osteoconduction, were compared with histology results for the experiments. A threshold was applied to display areas of bone with a minimum tissue density of 1 GPa [32]. Quarter slices of the FEA models were created by varying the angle of the cut in 10° increments (Fig. 2A), to replicate the histological cuts. For each histology slice, two FEA cuts with the closest plug pattern were selected. The FEA slices were imported into ImageJ, and converted to greyscale images for analysis. The extent of osteointegration for each slice was computed by measuring the length of the implant in contact with bone,

normalised by the total inner surface perimeter of the implant. The mean value was validated with the results reported by Mumith et al. [13]. Standard deviations were calculated using OriginPro 2016 (OriginLab Corp., Northampton, MA).

3. Results

3.1. Bone remodelling predictions

The remodelling patterns predicted for the uncoated cases were similar for both pore sizes (Fig. 3A, B). In the uncoated cases, bone ingrowth was limited to the circumference, around the outer pores and struts. The bone ingrowth was highest on top of the implant (loading direction), and decreases towards the sides. For the coated implants, when osteoconduction, together with osteoconnectivity, was modelled, bone formation reached the centre of the implant, surrounding all the the struts forming a thin layer of bone over the surface of the porous implant (Fig. 3C, D). However, the remodelling pattern within the centre of the pores remained similar to the uncoated cases with limited bone ingrowth. The use of conductivity caused the volume of bone formation to increase from 34% and 23% to 45% and 38%, for the 1500 and 700 μm plug sizes respectively. The average apparent density of the soft tissue increased from 0.75 to 0.79 gcm^{-3} and 0.66 to 0.73 gcm^{-3} for the larger and smaller pores respectively.
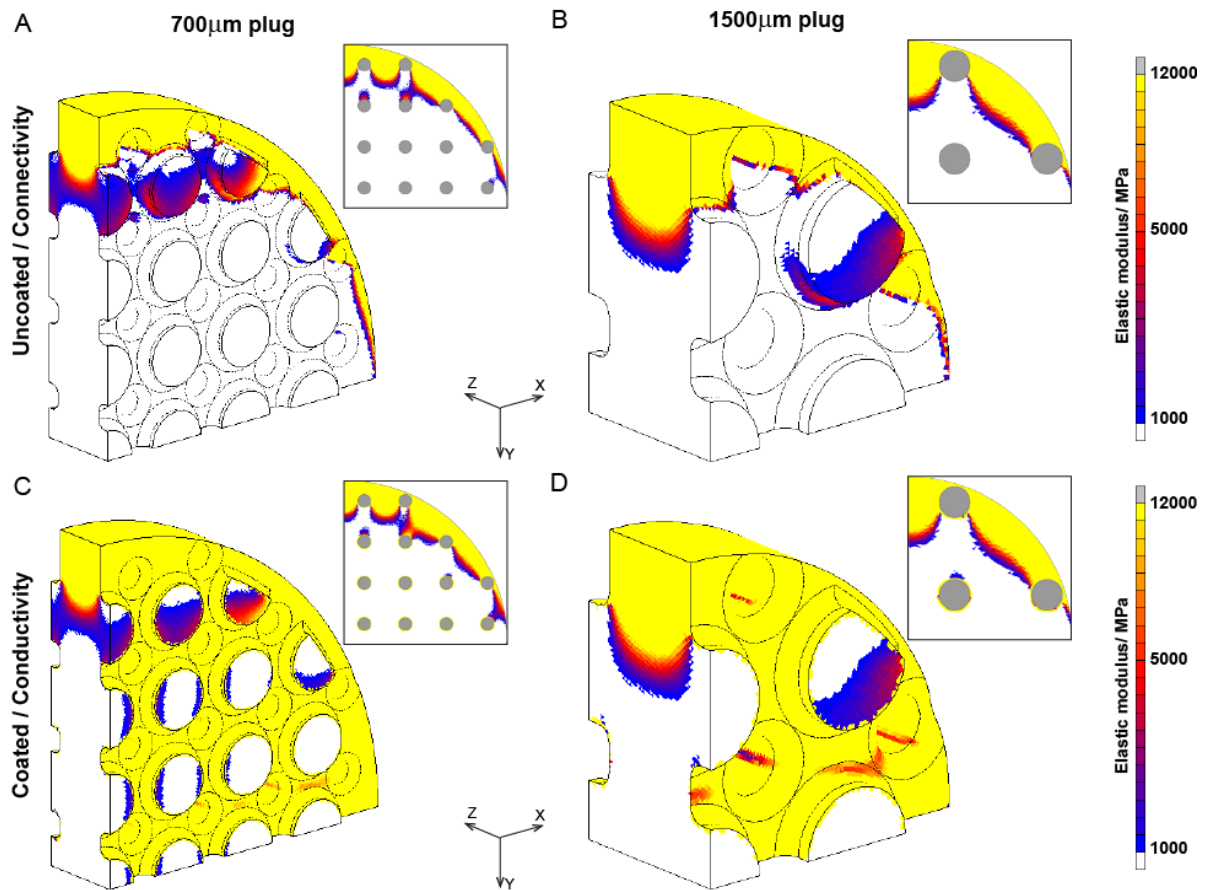
Fig. 3. 3D view of bone remodelling in soft tissue scaffold at equilibrium, with plate and bone removed for visualisation. (A) 700μm plug size, uncoated. (B) 1500μm plug size, uncoated. (C) 700μm plug size, coated with osteoconductive material. (D) 1500μm plug coated with osteoconductive material. Insets show cuts across pore (soft tissue) centre, with the location of the struts marked in grey.

Transverse cuts of the adaptive FEA models taken at 45° show the progression with time of bone remodelling from the bone (Fig. 4). For the uncoated 700 μm implant (Fig. 4A), bone remodelling was restricted to the outer pore. All tissue in the outer pore was remodelling at 10 ctu. The highest density (12 GPa), representing bone, was at the edge of the plates, in contact with the existing bone, while the least remodelling occurred around the fillet of the struts. Remodelling continued beyond 20 ctu until all the bone became fully dense. In the coated 700 μm model, remodelling and osteointegration of the outer pore occurred more rapidly than for the uncoated case at 10 ctu (Fig. 4C), leading to higher bone density. At 20 ctu, bone formation had progressed to the inner pores, along the coated surface of the plates and webs of the inner struts. At equilibrium, osteointegration

had occurred along all the implant surfaces. Bone ingrowth within the inner pores was limited to the coated implant surface.

For the uncoated 1500 μm model, the volume of bone formed and its density increased with time in the outer pore as it was not restricted by the location of the struts (Fig. 4B). At equilibrium, bone ingrowth just about reached the corner of the plates at the inner strut on the outer pore. Bone ingrowth showed a density gradient, with decreasing modulus towards the strut, unlike the homogenous bone density in the 700 μm model. The bone ingrowth pattern was similar in the coated 1500 μm implant (Fig. 4D). However, bone formed on the top of the inner plate and the web at 10 ctu before remodelling occurred at the fillet. At 20 ctu, remodelling spread to the underside of the inner web and plate, but also to the outer plates. At equilibrium, the elements adjacent to the coated implant have the highest densities. The main geometrical changes occurred by 36 ctu, and only changes in tissue density were observed thereafter. Increased bone growth was predicted for the FEA models that included osteoconductivity, where bone formed on the surface of struts deep within the porous implant.
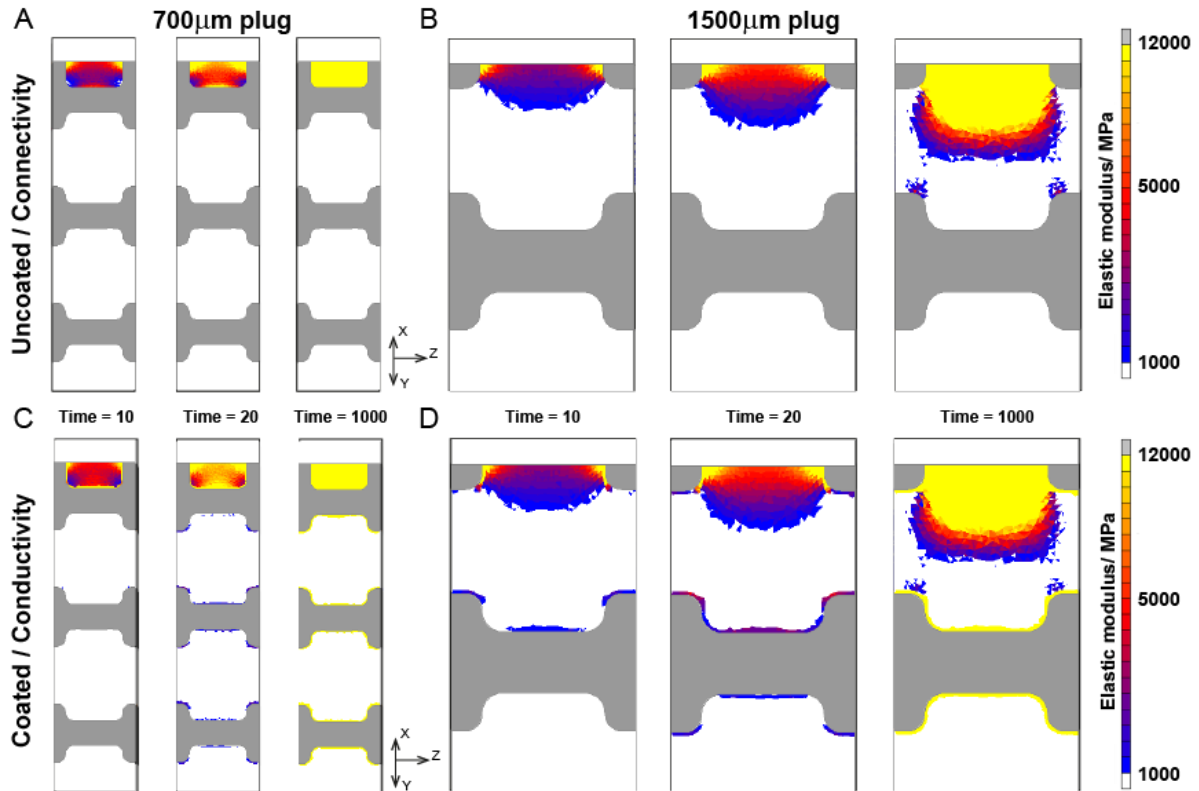
Fig. 4. Bone ingrowth into 45° transverse slice of a Ti6Al4V implant with time. (A) 700μm plug size, uncoated. (B) 1500μm plug size, uncoated. (C) 700μm plug size, coated with osteoconductive material. (D) 1500μm plug size, coated with osteoconductive material; grey: implant, white; soft tissue.

3.2. Verification of finite element simulations

Fig. 5 shows the qualitative comparison between the numerical results at equilibrium and the histology of the animal study. For the 700 μm cases, bone formation was observed in the outer pores of the implant for both the experimental and FEA results of coated and uncoated implants (Fig. 5A, C). For the uncoated implant (Fig. 5A), no bone ingrowth was predicted for the inner pores, corresponding well with the histology result. The 700 μm model with osteoconduction showed a thin layer of bone growth localised along the struts with a high degree of osteointegration, with some variations but overall similar to the histology results (Fig. 5C). This agreed well with both the histology and the backscattered scanning electron microscopy (BSEM) result of a coated 700 μm implant. The BSEM image shows the pores of the scaffold partially filled with lamellar bone attached to the implant coating (Fig. 6). The histology and SEM results suggest a thicker layer of bone

14

For the 1500 μm pore size, the simulations predicted a partial filling of the outer pore for both coated and uncoated cases, which appears slightly higher than observed from the histology results (Fig. 5B, D). The histology for the coated implant showed a layer of bone growth adjacent to the implant, which the conductivity model predicted well (Fig. 5D).
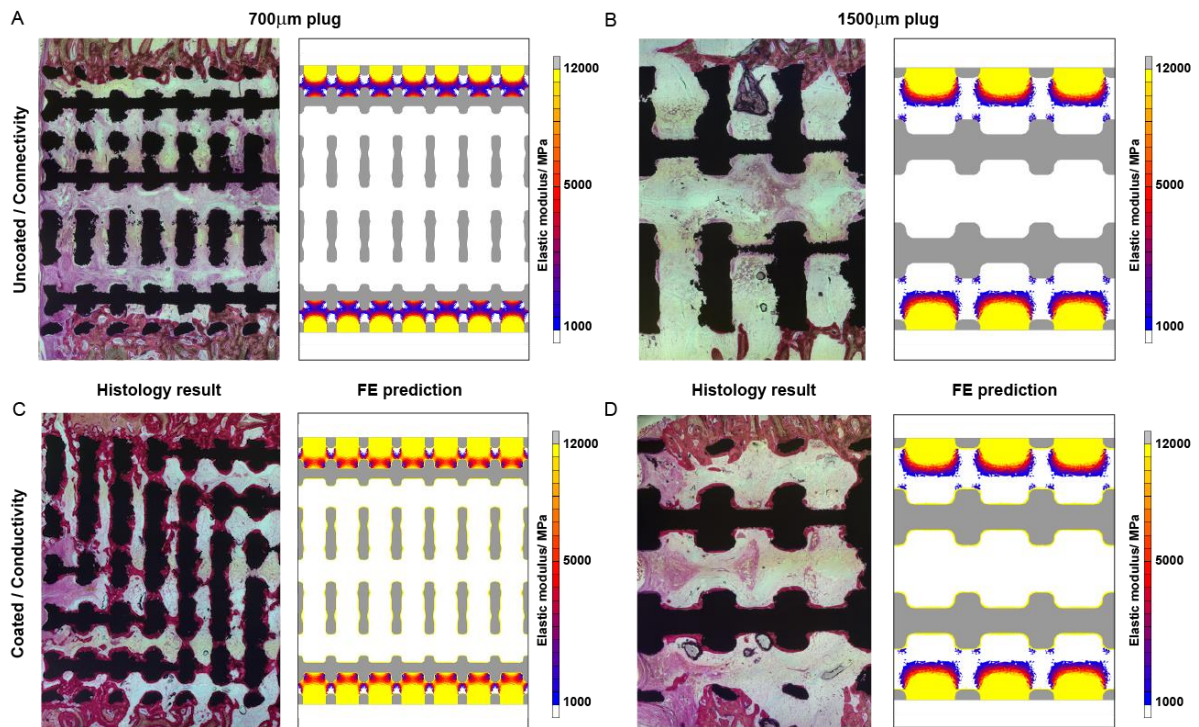

Fig. 5. Comparison of bone ingrowth between histology and numerical results in (A) 700 μm plug size, uncoated, (B) 1500 μm plug size, uncoated, (C) 700 μm plug size, HA-coated, and (D) 1500 μm plug size, HA-coated. Bone and soft tissue are stained red and pink in the histological analysis respectively.
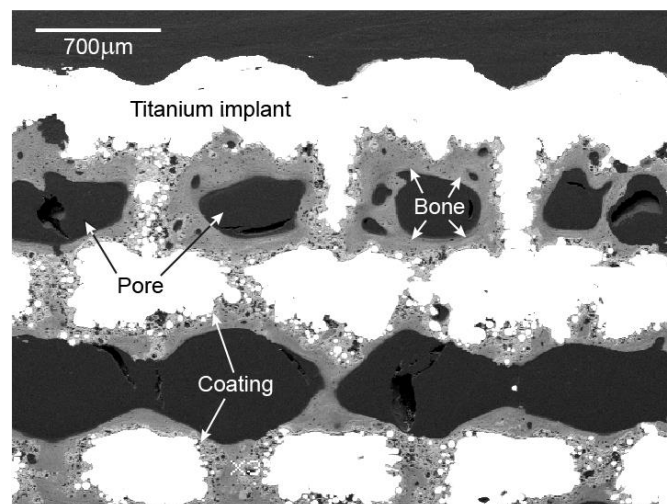
The extent of surface integration observed from the histology slices and predicted by the FEA simulations is compared in Fig. 7. From the histology results, similar levels of surface integration were found for both pore sizes of the uncoated implants at 10% and 11% for the 1500 and 700 µm implants respectively. Histology for the 1500 and 700 µm coated implants showed 75% and 80% of the pore surfaces osteointegrated respectively, which was significantly higher than the uncoated cases. No statistical significant difference between pore sizes was found. The FEA models predicted similar levels of bone growth of 19% and 23% of surface integration for the 1500 and 700µm uncoated plugs respectively, which is an over prediction by about 10%. For the coated models, the FEA results predicted a significantly higher amount of surface integration of 93% for the 1500 µm and 97% for the 700µm plug, approximately 15% higher than the histology results.
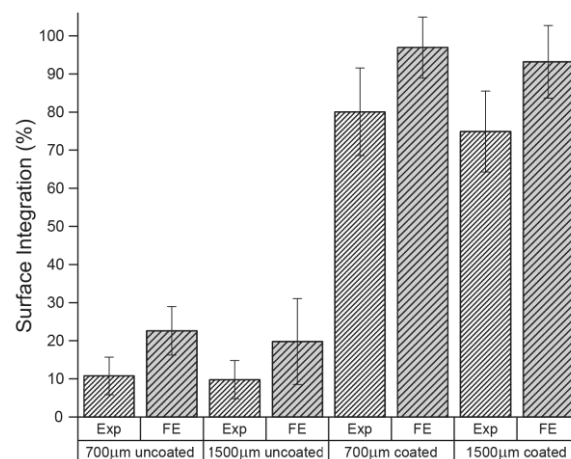

Fig. 7. Comparison of the extent of surface integration between the histology (Exp) and simulation (FEA) results. Error bars represent standard deviation.

3.3. Parametric variation of material properties

Fig. 8 shows the extent of bone ingrowth at equilibrium for varying material properties (stiffness) of the implant. The change from Ti6Al4V (110 GPa, Fig. 8A) to uncoated Ti-70%Ta alloy (67 GPa, Fig. 8B) showed an increase in ingrowth volume for the 700 µm case from 23% to 59%, with additional bone formation concentrated around the plates. The web of the inner struts exhibited some osteointegration, but not at the fillets or on the underside of the first strut. For the 1500µm

16

uncoated model, the increase in osteointegration was limited to the outer pore, leading to an increase in ingrowth from 34% to 56%. A region without bone ingrowth can be seen just above the second strut. The inclusion of osteoconduction for the 67 GPa material increased bone formation to 65% and 66% for the 700 and 1500 μm implants respectively. This corresponded to increased osteointegration along the coated surface, but there was additional ingrowth in the inner pore for the 1500 μm case (Fig. 8B). For an assumed implant material of 50 GPa stiffness (Ti-Ni), bone formation occurred in all pores, with additional ingrowth and denser bone compared to the Ti-70%Ta alloy. However, osteointegration and bone formation were absent directly below the first layer of struts for the 700 μm case (Fig. 8C). Osteoconduction increased ingrowth by less than 4%, leading to 92% and 79% bone volume for the 700 and 1500 μm implants respectively. Similar remodelling patterns were observed for the 40GPa material, but with increased ingrowth (not shown). Full ingrowth of dense bone throughout the porous implant was observed for both the coated and uncoated cases for PEEK (3.8 GPa) (Fig. 8D) and a 25 GPa material (not shown).
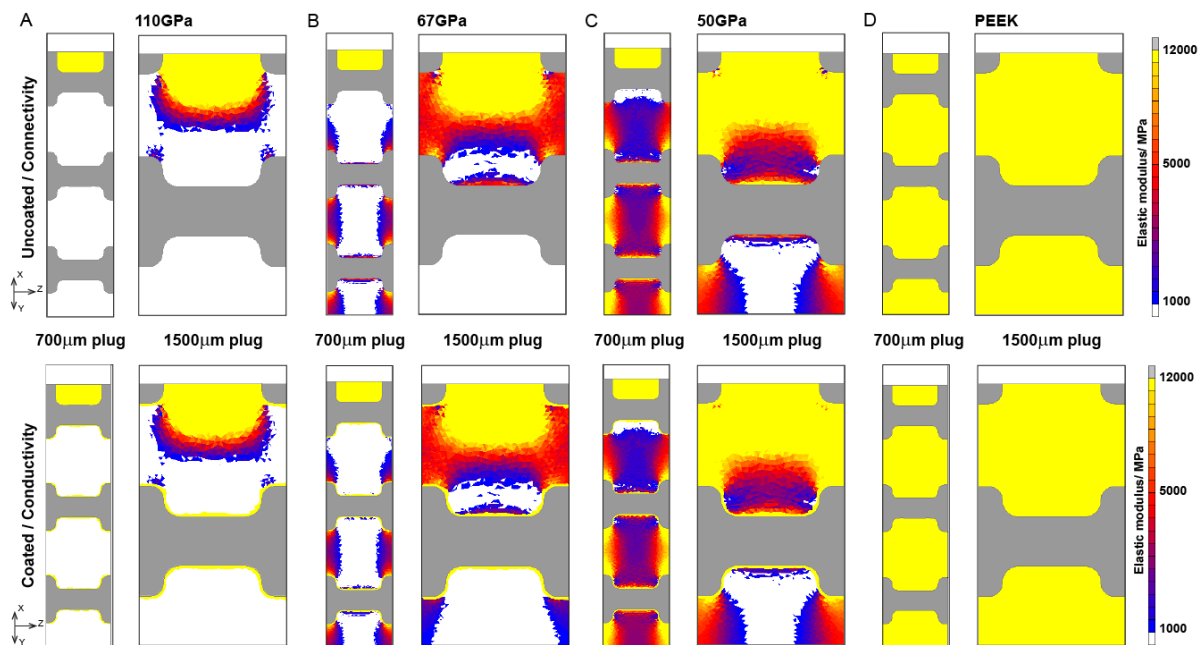

Fig. 8. Bone remodelling and osteointegration at equilibrium (1000 ctu) for different implant material properties (stiffness) and coating. (A) Ti6Al4V, 110GPa. (B) Ti-70%Ta, 67GPa. (C) Ni-Ti, 50GPa. (D) PEEK, 3.8GPa.

The remodelling curves for the 1500μm pore size show the change in average tissue density with computation time (Fig. 9). A decrease in the stiffness of the implant material increased the remodelling rate and led to higher average density. The amount and rate of bone formation was enhanced in the stiffer materials where osteoconductivity was applied, and led to a higher average tissue density at equilibrium. The contribution of the coating was largest for the two Titanium alloys as the final density increased by 5% to reach 0.79 and 0.92 gcm^{-3} for implants with material stiffness of 110 and 67 GPa respectively. Lowering the modulus decreased the contribution of osteoconduction. For 50 and 40 GPa materials, osteoconduction increased the average tissue density by 3% and 2% to reach 1.20 and 1.05 gcm^{-3} respectively. For the 25 GPa material, the tissue density converged to 1.41 gcm^{-3} at equilibrium for the uncoated case. The addition of osteoconduction increased the density by 0.6%. For PEEK, the tissue density saturated at 1.47 gcm^{-3} for both the uncoated and coated cases, the upper limit set for bone density.
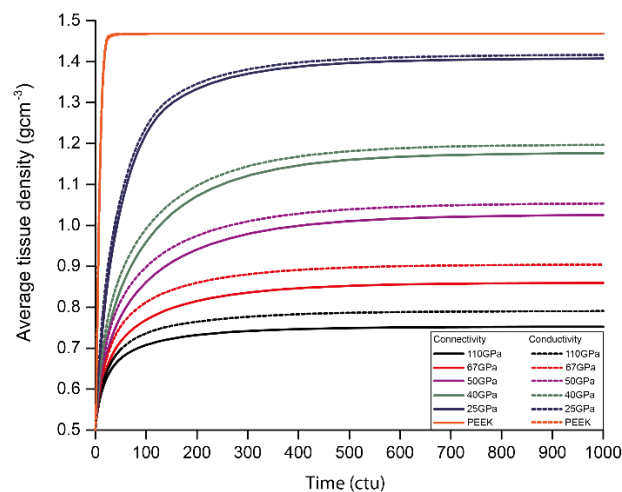

Fig. 9. Change in average tissue density with time for different implant material properties (stiffness) and the influence of HA-coating (osteconductivity) for 1500 μm sized plugs.

4.   Discussion

In this study, finite element simulations were combined with new algorithms to model bone ingrowth (osteoconnectivity) and the effect of surface modification on osteoconduction, in order to predict bone ingrowth into porous titanium implants. The numerical results were verified against histology from animal models, where bone ingrowth and osteointegration were measured. The

effect of an osteoconductive coating was to induce bone formation along the inner porous surface, but this only added marginally to the levels of bone ingrowth. There was an effect of the pore geometry on bone ingrowth and a more open pore structure adjacent to the original bone interface is advocated.

Porous titanium alloys have recently been manufactured by foaming and sintering, producing interconnected pores and a complex surface topography to enhance bone ingrowth [33]. However, it is difficult to alter the size of the pores and optimise the geometry of the prosthesis with these materials [27]. The use of selective laser sintering in the manufacture of titanium alloy prostheses allows functionally graded porosity to be used in a single prosthesis. In order to provide the appropriate strength, these may be joined to solid metal made by the same process. However it is unclear if the rules associated with bone ingrowth on surfaces of conventional implants apply to implants which are substantially more porous.

A recent method to design scaffolds utilised computed tomography (CT), mechanical testing, and statistical analysis to predict the effects of pore size, porosity, strut thickness, and topology on the elastic modulus and compressive yield strength of additively manufactured porous biomaterials [34]. Whilst this approach is extremely valuable to minimize the mismatch in the structural stiffness of the implant to the bone [7], it does not relate the porous structure to the level of bone ingrowth and osteointegration. At present, it is unclear if the shape and size of pores used to construct implants can be optimised for bone ingrowth, as the literature reports contradictory results. De Wild et al. [35] used 5 different lattice designs with pore sizes between 700 and 1300 μm and showed the maximum of bone ingrowth to be below 40% and not significantly different between the designs, in noncritical-sized defect bridging in calvarial bones of rabbits. However, octet-truss structure was shown to cause more ingrowth than tetrahedron structures in canine femurs [7]. Moreover, an animal study has shown localised and limited bone ingrowth, demonstrating that it is insufficient to

assume the occurrence of osteointegration throughout the implant in the optimisation of design [27].

Histological analysis conducted on uncoated porous 700 and 1500 μm plugs implanted in ovine condylar defect models after 6 weeks showed the amount of osteointegration (at a level of 10% of the available surface) was similar and independent of pore size [13]. Osteointegration increased to above 75% when the implants were HA coated. The FEA models use SED as the driver for remodelling and were verified with the histology results, predicting similar amounts of osteointegration for the uncoated plugs for both pore sizes (Fig. 4). Modelling osteoconduction predicted a significant increase in osteointegration for the coated models, in line with the histology results. The simulated bone remodelling patterns were similar to the histology results with bone ingrowth limited to the outer pores for the uncoated cases, and osteointegration observed along the coated surfaces (Fig. 5). The FEA remodelling results showed limited bone ingrowth into inner pores, even when the implants were HA-coated. While the use of a biomimetic coating increased osteointegration significantly, ingrowth remained less than 50% and bone formation was localised around the coated struts (Fig. 6). These remodelling patterns are caused by stress shielding of the Ti6Al4V struts, which lowers SED in the inner pores. Coating porous Ti6Al4V enhanced osteointegration of the inner pores surfaces, but did not promote significant bone ingrowth.

The limited bone growth in the inner pores as predicted by the FEA models agrees with results from studies that have evaluated bone ingrowth in animals using similar non-flexible, uncoated implant designs [27, 36, 37]. The 23% ingrowth predicted in the 700 μm model (300 μm strut size, 75% porosity) is consistent with the reported ingrowth of 19.23 ± 6.39% in a cylindrical implant 7.5mm in diameter (strut size of 200 μm, cross section 700 x 700 μm and 83.5% porosity), after 8 weeks in non-critical sized defects in calvarial rabbit bone [36]. The 34% ingrowth predicted in the 1500 μm model is higher than ingrowth of 15 − 28% obtained using a 53% porous structure with pore sizes

between 800 and 1500 μm in sheep mandibles [37], but is within the range of ingrowth reported in porous scaffolds [27].

The developed FEA models consistently overestimated the amount of osteointegration by about 10 – 15%. This could be due to limitations of the models or biological reasons. The FEA model was developed as a quarter slice by exploiting symmetry and repeating pattern of the implant design. This assumed that the slice is located away from the implant edges. The FEA prediction in Fig. 5 is a reconstruction from repeating slices and shows the locations where remodelling could occur, which does not happen perfectly as the biological response is subject-specific and multifactorial. The orientation of the implant may also be rotated during surgery but the FEA model here represented the case with the highest amount of ingrowth. The histology results were obtained at 6 weeks, and were compared with equilibrium FEA results. It is also possible that bone remodelling in the implants in the ovine model had not reached equilibrium.

The ingrowth across the middle of the struts was highest in the loading direction, but remodelling volume was limited to the outer struts (Fig. 3 insets). Bone formation occurred in pores near the first column of struts for the 700 μm implant, which was absent in the 1500 μm implant. This could be caused by the slightly higher load/volume ratio of 700 μm implant, resulting in more load transfer to the soft tissue. The bone formed in the outer pore was fully dense for the 700 μm implant, without a density gradient that penetrated further in the 1500 μm case (Fig. 4, 8). Moreover, the extent of osteointegration (Fig. 5) depends on the surface area available. The higher surface area to volume ratio for the 700 than for the 1500 μm implant suggests that the former should have exhibited a higher amount of osteointegration even in the uncoated case. These result suggests that the placement of the outer layer of struts is critical in optimising the extent of osteointegration, depending on the material used; the smaller plug size would benefit from struts located nearer the centre of the implant. Nevertheless, the advantage with the current 700 μm model is improved mechanical interlock due to full osteointegration at the outer pores. Therefore, moving the location

of the struts of the 1500 μm implant towards the circumference of the implant could improve osteointegration without sacrificing bone ingrowth.

The results showed stress shielding of conventional titanium alloy due to material stiffness and implant geometry, limiting ingrowth and osteointegration. Assessment of the influence of a reduction in the apparent mechanical properties of fully load-bearing porous titanium implants in mandibular bone defects indicated the importance of lower modulus porous structures to promote increased bone ingrowth [37]. To improve bone ingrowth in the implant, materials with lower modulus were investigated to reduce stress shielding (Fig. 8). Simulations for reduced implant material stiffness predicted increased bone ingrowth. Good results were predicted for the use of uncoated Titanium-tantalum alloy Ti-70%Ta, as ingrowth was predicted to exceed 50% for both pore sizes. The ingrowth into the inner pores of the 700 μm implant suggests that its structural stiffness is slightly lower than that of the 1500 μm implant. The use of osteoconduction caused bone ingrowth into the inner pores of the 1500 μm model, suggesting that the SED was initially borderline below the threshold. The regions without bone ingrowth, located above the struts in the 1500 μm model, suggest that stress shielding imposes an important effect. Although coating had a significant effect on bone formation on the surface of the inner pores, they were never completely filled in with bone in conventional titanium alloy for both pore sizes investigated, again suggesting that stress shielding imposes an important effect. In the FEA model, the use of PEEK allowed the formation of fully dense bone, as its material stiffness is similar to that of bone. Investigating different modulus values for hypothetical materials between titanium alloy and PEEK demonstrated increased ingrowth and remodelling rate, due to increased load distribution on the soft tissue associated with a reduction in stress shielding (Fig. 9). Very good ingrowth was predicted for moduli between 40 – 50 GPa, but no such material at the present time exists which can be used for the manufacture of implants by 3D additive manufacturing methods.

The contribution of an osteoconductive coating to ingrowth was the highest on the 1500 μm 67 GPa implant and promoted bone formation in the inner pores, marginally higher than that for the 700 μm case. However, the contribution of osteoconduction reduces with decreasing modulus, as the driver for bone remodelling increase and osteoconduction does not lead to additional bone ingrowth into the middle of the pores. The use of coating in lower modulus materials only increased the densification of tissues adjacent to the implant, but this contribution became insignificant when full ingrowth was achieved below a material stiffness of 25GPa.

Biologically, PEEK is not as effective as titanium and titanium alloys in promoting osteointegration, nevertheless, complete bone ingrowth would lead to mechanical interlock, which is beneficial for load transfer. The saturation of the tissue density for PEEK in Fig. 9 is the result of the threshold placed on the remodelling of bone, to prevent unrealistic bone density from forming. Histological analysis yields no information about the quality of the bone formed in the implants, and given that the plugs were implanted in the condyles and surrounded by trabecular bone, it was necessary to limit the density of the bone formed. As titanium-based alloys are known to enable bone formation on their surface [36] and for this reason osteointegration of bone with the implant was assumed when remodelling of bone occurred adjacent to the implant. Two limitations of this study are that the tissue density of the thin layer of bone formed on the coated implants (Fig. 6) was not quantified and that bone volume formation was not measured in 3D. Micro-CT scans can be conducted to obtain the volume of bone formation within a specific region of interest (ROI) to compare the performance of different bone implants [27, 37]. It has been reported that measuring bone morphology a distance of 1mm away from the surface of the implant caused little artefact [27]. The pore sizes used in this study were 1000 microns and below, and the bone formed on the coated implants was rather thin and localised (Fig. 5, 6), which would lead to imaging artefacts. For different implant designs with thicker layers of bone formation, bone morphometric analysis via micro-CT scans could be conducted [27]. The histology and SEM results suggest a thicker layer of bone formation at the surface of the coated implants than predicted by the FEA. Further work should

explore the use of novel imaging techniques, such as ultrasound spectroscopy or nano-CT, to quantify the quality of bone growth at different time points, to refine the algorithm and for the computation time units in the FEA model to be correlated with bone formation in real time. Geometrical changes to the design of the implant could be investigated while assessing their long-term fatigue strength and failure strain.

5.   Conclusion

The developed Finite Element models were able to predict the level of osteointegration and bone ingrowth into porous implants, which are based on two novel algorithms that modelled the sequential laying down of bone and the effect of osteoconductive coating. The limited bone ingrowth into the pores was found to be due to the stress shielding of the stiff outer struts of the implant, leading to low strain energy density in the inner implant pores. Significantly increased osteointegration was observed along the implant surfaces coated with HA, but only a small increase of overall bone ingrowth. Finite Element simulations for lower implant material stiffness predicted significantly increased bone ingrowth for Ti-70%Ta, a Titanium alloy with lower elastic modulus. In combination with an osteoconductive coating, good osteointegration and bone ingrowth was predicted. Further improvements could be achieved by lowering the stiffness of the implant, either using materials with lower elastic modulus or through changes to the implant design. The algorithms developed in this study could be used to design substantially porous implants, predicting bone ingrowth. Empirical designs based on bone formation in animal studies could be optimised prior to testing *in vivo*. The verification of these FEA models was utilised in an *in vivo* model but the loads and forces associated with implants in human could be used with these algorithms to investigate more functional, substantially porous implants in humans.

Acknowledgements

References

[1] G. Blunn, M. Coathup, Fixation of Endoprostheses in Tumour Replacement, European Surgical Orthopaedics and Traumatology, Springer2014, pp. 4119-4133.

[2] E.Y. Chao, F.H. Sim, Composite fixation of salvage prostheses for the hip and knee, Clin. Orthop. Relat. Res. 276 (1992) 91-101.

[3] M.J. Coathup, V. Batta, R.C. Pollock, W.J. Aston, S.R. Cannon, J.A. Skinner, T.W. Briggs, P.S. Unwin, G.W. Blunn, Long-term survival of cemented distal femoral endoprostheses with a hydroxyapatite-coated collar: a histological study and a radiographic follow-up, J. Bone Joint Surg. Am. 95(17) (2013) 1569-75.

[4] P. Fromme, G.W. Blunn, W.J. Aston, T. Abdoola, J. Koris, M.J. Coathup, The Effect of Bone Growth onto Massive Prostheses Collars in Protecting the Implant from Fracture, Med. Eng. Phys. 41 (2017) 19-25.

[5] M. Fini, G. Giavaresi, P. Torricelli, V. Borsari, R. Giardino, A. Nicolini, A. Carpi, Osteoporosis and biomaterial osteointegration, Biomed. Pharmacother. 58(9) (2004) 487-493.

[6] M. Long, H.J. Rack, Titanium alloys in total joint replacement—a materials science perspective, Biomaterials 19(18) (1998) 1621-1639.

[7] S. Arabnejad, B.R. Johnston, J.A. Pura, B. Singh, M. Tanzer, D. Pasini, High-strength porous biomaterials for bone replacement: A strategy to assess the interplay between cell morphology, mechanical properties, bone ingrowth and manufacturing constraints, Acta Biomater. 30 (2016) 345-56.

[8] X. Li, Y.F. Feng, C.T. Wang, G.C. Li, W. Lei, Z.Y. Zhang, L. Wang, Evaluation of biological properties of electron beam melted Ti6Al4V implant with biomimetic coating in vitro and in vivo, PLoS One 7(12) (2012) e52049.

[9] S.L. Sing, W.Y. Yeong, F.E. Wiria, Selective laser melting of titanium alloy with 50 wt% tantalum: Microstructure and mechanical properties, J. Alloys Compd. 660 (2016) 461-470.

[10] P. Laheurte, F. Prima, A. Eberhardt, T. Gloriant, M. Wary, E. Patoor, Mechanical properties of low modulus beta titanium alloys designed from the electronic approach, J. Mech. Behav. Biomed. Mater. 3(8) (2010) 565-73.

[11] F. Barrère, C.M. van der Valk, G. Meijer, R.A.J. Dalmeijer, K. de Groot, P. Layrolle, Osteointegration of biomimetic apatite coating applied onto dense and porous metal implants in femurs of goats, J. Biomed. Mater. Res. B Appl. Biomater. 67B(1) (2003) 655-665.

[12] J. Redepenning, T. Schlessinger, S. Burnham, L. Lippiello, J. Miyano, Characterization of electrolytically prepared brushite and hydroxyapatite coatings on orthopedic alloys, J. Biomed. Mater. Res. A 30(3) (1996) 287-294.

[13] A. Mumith, G. Blunn, V.S. Cheong, P. Fromme, M. Coathup, Bone growth within a 3D printed porous scaffold is driven by osteoconductive coatings and not pore size, Eur Cells Mater (in review).

[14] A. Mumith, M. Coathup, M. Chimutengwende-Gordon, W. Aston, T. Briggs, G. Blunn, Augmenting the osseointegration of endoprostheses using laser-sintered porous collars: an in vivo study, Bone & Joint J. 99-B(2) (2017) 276-282.

[15] R. Hedayati, S. Janbaz, M. Sadighi, M. Mohammadi-Aghdam, A.A. Zadpoor, How does tissue regeneration influence the mechanical behavior of additively manufactured porous biomaterials?, J. Mech. Behav. Biomed. Mater. 65 (2017) 831-841.

[16] A. Dickinson, A. Taylor, M. Browne, Implant-bone interface healing and adaptation in resurfacing hip replacement, Comput. Methods Biomech. Biomed. Engin. 15(9) (2012) 935-47.

[17] X. Liu, G.L. Niebur, Bone ingrowth into a porous coated implant predicted by a mechano-regulatory tissue differentiation algorithm, Biomech. Model Mechanobiol. 7(4) (2008) 335-44.

[18] A.A. Zadpoor, J. Malda. Additive Manufacturing of Biomaterials, Tissues, and Organs. *Ann. Biomed. Eng.* 45(1) (2017) 1-11.

[19] R. Huiskes, H. Weinans, H. Grootenboer, M. Dalstra, B. Fudala, T. Slooff, Adaptive bone-remodeling theory applied to prosthetic-design analysis, J. Biomech. 20(11-12) (1987) 1135-1150.

[20] H. Weinans, R. Huiskes, H. Grootenboer, The behavior of adaptive bone-remodeling simulation models, J. Biomech. 25(12) (1992) 1425-1441.

[21] R.T. Hart, D. Davy, K. Heiple, A computational method for stress analysis of adaptive elastic materials with a view toward applications in strain-induced bone remodeling, J. Biomech. Eng. 106(4) (1984) 342-350.

[22] M. Tarala, D. Janssen, N. Verdonschot, Balancing incompatible endoprosthetic design goals: a combined ingrowth and bone remodeling simulation, Medical Engineering and Physics 33(3) (2011) 374-80.

[23] P.K. Tomaszewski, N. Verdonschot, S.K. Bulstra, J.S. Rietman, G.J. Verkerke, Simulated bone remodeling around two types of osseointegrated implants for direct fixation of upper-leg prostheses, J. Mech. Behav. Biomed. Mater. 15 (2012) 167-75.

[24] K. Mukherjee, S. Gupta, Bone ingrowth around porous-coated acetabular implant: a three-dimensional finite element study using mechanoregulatory algorithm, Biomech. Model Mechanobiol. 15(2) (2016) 389-403.

[25] V.S. Cheong, G. Blunn, M. Coathup, P. Fromme, Adaptive 3D Finite Element Analysis Model to Simulate Extracortical Bone Growth, Comput. Methods Biomech. Biomed. Eng. 21(2) (2018) 129-138.

[26] H. Kang, J.P. Long, G.D.U. Goldner, S.A. Goldstein, S.J. Hollister, A paradigm for the development and evaluation of novel implant topologies for bone fixation: implant design and fabrication, J. Biomech. 45(13) (2012) 2241-2247.

[27] J.P. Long, S.J. Hollister, S.A. Goldstein, A paradigm for the development and evaluation of novel implant topologies for bone fixation: In vivo evaluation, J. Biomech. 45(15) (2012) 2651-2657.

[28] W.R. Taylor, R.M. Ehrig, M.O. Heller, H. Schell, P. Seebeck, G.N. Duda, Tibio-femoral joint contact forces in sheep, J. Biomech. 39(5) (2006) 791-8.

[29] Y.L. Zhou, M. Niinomi, T. Akahori, Effects of Ta content on Young's modulus and tensile properties of binary Ti–Ta alloys for biomedical applications, Mater. Sci. Eng. A 371(1-2) (2004) 283-290.

[30] S. Cowin, D. Hegedus, Bone remodeling I: theory of adaptive elasticity, J. Elast. 6(3) (1976) 313-326.

[31] D. Carter, W. Hayes, The compressive behavior of bone as a two-phase porous structure, J. Bone Joint Surg. Am. 59(7) (1977) 954-962.

[32] R.B. Ashman, J.Y. Rho, Elastic modulus of trabecular bone material, J. Biomech. 21(3) (1988) 177-181.

[33] R.M. Wazen, L.P. Lefebvre, E. Baril, A. Nanci, Initial evaluation of bone ingrowth into a novel porous titanium coating, J. Biomed. Mater. Res. B Appl. Biomat. 94(1) (2010) 64-71.

[34] D. Melancon, Z. Bagheri, R. Johnston, L. Liu, M. Tanzer, D. Pasini, Mechanical characterization of structurally porous biomaterials built via additive manufacturing: experiments, predictive models, and design maps for load-bearing bone replacement implants, Acta Biomater. 63 (2017) 350-368.

[35] M. de Wild, S. Zimmermann, J. Rüegg, R. Schumacher, T. Fleischmann, C. Ghayor, F.E. Weber, Influence of Microarchitecture on Osteoconduction and Mechanics of Porous Titanium Scaffolds Generated by Selective Laser Melting, 3D Print. Addit. Manuf. 3(3) (2016) 142-151.

[36] M. de Wild, R. Schumacher, K. Mayer, E. Schkommodau, D. Thoma, M. Bredell, A. Kruse Gujer, K.W. Grätz, F.E. Weber, Bone regeneration by the osteoconductivity of porous titanium implants manufactured by selective laser melting: a histological and micro computed tomography study in the rabbit, Tissue Eng. Part A 19(23-24) (2013) 2645-2654.

[37] T. Schouman, M. Schmitt, C. Adam, G. Dubois, P. Rouch, Influence of the overall stiffness of a load-bearing porous titanium implant on bone ingrowth in critical-size mandibular bone defects in sheep, J. Mech. Behav. Biomed. Mater. 59 (2016) 484-496.